

ARTICLE

Excitation–Contraction Coupling

Superfast excitation–contraction coupling in adult zebrafish skeletal muscle fibers

 Romane Idoux¹ , Sandrine Bretaud² , Christine Berthier¹ , Florence Ruggiero² , Vincent Jacquemond¹ , and Bruno Allard¹ 

The zebrafish has emerged as a very relevant animal model for probing the pathophysiology of human skeletal muscle disorders. This vertebrate animal model displays a startle response characterized by high-frequency swimming activity powered by contraction of fast skeletal muscle fibers excited at extremely high frequencies, critical for escaping predators and capturing prey. Such intense muscle performance requires extremely fast properties of the contractile machinery but also of excitation–contraction coupling, the process by which an action potential spreading along the sarcolemma induces a change in configuration of the dihydropyridine receptors, resulting in intramembrane charge movements, which in turn triggers the release of Ca^{2+} from the sarcoplasmic reticulum. However, thus far, the fastest Ca^{2+} transients evoked by vertebrate muscle fibers has been described in muscles used to produce sounds, such as those in the toadfish swim bladder, but not in muscles used for locomotion. By performing intracellular Ca^{2+} measurements under voltage control in isolated fast skeletal muscle fibers from adult zebrafish and mouse, we demonstrate that fish fast muscle fibers display superfast kinetics of action potentials, intramembrane charge movements, and action potential–evoked Ca^{2+} transient, allowing fusion and fused sustained Ca^{2+} transients at frequencies of excitation much higher than in mouse fast skeletal muscle fibers and comparable to those recorded in muscles producing sounds. The present study is the first demonstration of superfast kinetics of excitation–contraction coupling in skeletal muscle allowing superfast locomotor behaviors in a vertebrate.

Introduction

In vertebrate skeletal muscle fibers, trains of action potentials spreading along the sarcolemma and transverse tubules trigger the release of Ca^{2+} from sarcoplasmic reticulum (SR) which activates contraction. The excitation–contraction (EC) coupling process corresponds to the series of events occurring between action potentials propagation and SR Ca^{2+} release (Allard, 2018). During this process, action potentials activate the dihydropyridine receptor (DHPR) anchored in the T-tubule membrane, which in turn opens the ryanodine receptor (RyR), a Ca^{2+} release channel anchored in the SR membrane. These two key proteins directly interact in skeletal muscle, implying that SR Ca^{2+} fluxes are under the tight control of muscle membrane voltage and that SR Ca^{2+} release and ensuing contraction occur a few milliseconds after excitation (Rios and Pizarro, 1991; Melzer et al., 1994; Schneider, 1994). In vertebrates, skeletal muscle fibers of slow and fast types are used at variable speeds and frequencies

to perform a wide range of locomotor activities (Schiaffino and Reggiani, 2011). Differences in the contraction kinetics between slow-twitch and fast-twitch skeletal muscle fibers result not only from differences in contractile proteins but also from differences in EC coupling kinetics, especially in the time course of action potential–evoked intracellular Ca^{2+} transients (Baylor and Hollingworth, 2012). The fastest EC coupling properties have, however, not been described in fast-twitch muscles used for locomotion but in muscles used to produce sounds (Rome, 2006). The Ca^{2+} transient evoked by muscle fibers from swim bladder of male toadfish that produce sounds when contracting during the mating call is indeed the fastest ever measured for any fiber type (Rome et al., 1996). Yet, the zebrafish *Danio rerio*, a very relevant vertebrate animal model for human muscle diseases (Guyon et al., 2007; Berger and Currie, 2012; Gibbs et al., 2013), has been shown to exhibit startle or escape response

¹Institut de Physiopathologie et Génétique du Neuron et du Muscle (PGNM), Université de Lyon, Université Claude Bernard Lyon 1, Centre National de la Recherche Scientifique UMR 5261, INSERM U1315, Faculté de Médecine Rockefeller, Lyon, France; ²Institut de Génomique Fonctionnelle de Lyon (IGFL), École normale supérieure de Lyon, Université Claude Bernard Lyon 1, Centre National de la Recherche Scientifique UMR 5242, Lyon, France.

Correspondence to Bruno Allard: bruno.allard@univ-lyon1.fr

This work is part of a special issue on excitation–contraction coupling.

© 2022 Idoux et al. This article is distributed under the terms of an Attribution–Noncommercial–Share Alike–No Mirror Sites license for the first six months after the publication date (see <http://www.rupress.org/terms/>). After six months it is available under a Creative Commons License (Attribution–Noncommercial–Share Alike 4.0 International license, as described at <https://creativecommons.org/licenses/by-nc-sa/4.0/>).

characterized by maximal tail beat and swimming activity frequencies up to 100 Hz and 50 Hz in larvae and adult, respectively (Buss and Drapeau, 2001; Müller and van Leeuwen, 2004; Kyriakatos et al., 2011). Measurements of muscle force on whole zebrafish larvae have also shown astonishing fast kinetics of twitches and extremely high fusion frequency of contraction, both much larger than those measured in mammalian and frog fast muscle fibers and close to those recorded in swim bladder muscle fibers (Dou et al., 2008). Such a fast phenotype should require extremely fast properties of EC coupling. However, although Ca^{2+} signals, action potentials and intramembrane charge movements have been recorded in zebrafish fast skeletal muscle cells, there was no attempt to compare kinetics with mammalian fast fibers (Buckingham and Ali, 2004; Schredelseker et al., 2005; Walogorsky et al., 2012; Robin and Allard, 2015; Linsley et al., 2017). Moreover, experiments have been performed on cultured myotubes, in situ or on isolated fibers exclusively from zebrafish at larval stage. Yet, number of muscle pathologies worsen with age or come up at ages far beyond embryonic stages, so that the use of zebrafish larvae to model those kinds of muscle disorders is limited. Additionally, it is known that zebrafish undergo profound metamorphosis at 3–4 wk of age that may result in important changes in the musculature (Parichy et al., 2009).

In the present study, we have been able to implement current- and voltage-clamp combined with intracellular Ca^{2+} measurements to provide a comprehensive characterization of EC coupling properties of isolated fast muscle fibers from adult zebrafish. We demonstrate that adult zebrafish fast muscle fibers display superfast kinetics of action potentials, intramembrane charge movements that reflect the change in configuration of the DHPR and action potential-evoked Ca^{2+} transients. Such superfast kinetics allow fusion and fused sustained Ca^{2+} transients at frequencies of excitation much higher than in mouse fast muscle fibers. The present study is the first demonstration of kinetics of EC coupling in skeletal muscle used for locomotion as fast as those described in muscles used to produce sounds (Nelson et al., 2014).

Materials and methods

Isolation and preparation of zebrafish and mouse muscle fibers

Zebrafish (AB/TU) were raised at 28.5°C and bred according to standard procedures (PRECI, SFR Biosciences UAR3444/CNRS, US8/Inserm, ENS de Lyon, UCBL, agreement number C693870602). All animal manipulations were performed in agreement with EU Directive 2010/63/EU. Male 11–13-mo-old zebrafish were euthanized with 0.3 g/liter tricaine (MS222; Sigma-Aldrich), decapitated, and skin was removed. Dorsal trunk muscle of around 3-mm width located just under the dorsal fin were removed and incubated for 40 min at 37°C in the presence of Tyrode solution containing 2 mg/ml of collagenase (Sigma-Aldrich, type 1). Single intact muscle fibers were then released by gentle mechanical trituration of the enzyme-treated muscles in a glass-bottomed experimental chamber, in the presence of culture medium containing 2% Matrigel (Sigma-Aldrich).

Experiments on mice were performed following the ethics principles of the French Department of Veterinary Services and the French Ministry for Higher Education, Research and Innovation, in accordance with the guidelines of the local animal ethics committee at University Claude Bernard Lyon 1 (Animal Experimentation Committee no. CEEA-015), the French Ministry of Agriculture (decree 87/848), and the revised European Directive 2010/63/EU. Adult male OF1 mice were killed by cervical dislocation before the removal of interosseal muscles. Single fibers were isolated by a 50-min enzymatic treatment at 37°C using a Tyrode solution containing 2-mg/ml collagenase type I (Sigma-Aldrich). Single intact muscle fibers were then released by gentle mechanical trituration of the enzyme-treated muscles in a glass-bottomed experimental chamber, in the presence of culture medium.

Electrophysiology

Prior to trituration, the bottom of the experimental chamber was covered with a thin layer of silicone grease. This enabled single fibers from zebrafish or mouse to be covered with additional silicone, so that a 50–100- μm -long portion of the fiber extremity was left out, as previously described (Idoux et al., 2020). The culture medium solution was replaced by the extracellular solutions (see Solutions). The tip of a glass micropipette filled with an intracellular-like solution containing a Ca^{2+} -sensitive dye (see Intracellular Ca^{2+} measurements) was inserted into the silicone-embedded fiber portion. The silver-silver chloride wire inside the micropipette was connected to an RK-400 patch-clamp amplifier (Bio-Logic) used in whole-cell voltage-clamp or current-clamp configuration. Command voltage or current pulse generation was achieved with an analog-digital converter (Digidata 1322A; Axon Instruments) controlled by pClamp 9 software (Axon Instruments). The tip of the micropipette was gently crushed against the bottom of the chamber to reduce the series resistance and to allow internal dialysis of the fiber. Current and voltage changes were acquired at a sampling frequency of 10 and 50 kHz, respectively.

Charge movement currents were calculated using conventional procedures consisting of subtracting scaled control current recorded in response to a 10-mV hyperpolarizing pulse from the current elicited by test depolarizing pulses of identical duration and of various amplitudes from a holding potential of -80 mV. Charge movement was quantified by integrating the transient outward current after the onset of the test pulse (Q_{on}) and subsequently normalized to cell capacitance ($\text{nC}/\mu\text{F}$). All experiments were performed at room temperature (20–22°C).

In current clamp experiments, the resting membrane potential of mouse and zebrafish muscle fibers was maintained at -100 mV by passing a constant hyperpolarizing current, because such a resting potential was required to ensure action potential firing in all zebrafish muscle fibers.

Intracellular Ca^{2+} measurements

Prior to voltage-clamp, the indo-1 dye, diluted at a concentration of 0.2 mM in an intracellular-like solution (see Solutions), was dialyzed into the fiber cytoplasm through the microelectrode inserted through the silicone, within the insulated part of the

fiber. Intracellular equilibration of the solution was allowed for a period of 20 min before initiating measurements. Indo-1 fluorescence was measured on an inverted Nikon Diaphot epifluorescence microscope equipped with a commercial optical system, allowing the simultaneous detection of fluorescence at 405 nm (F405) and 485 nm (F485) by two photomultipliers (IonOptix) upon 360-nm excitation. Background fluorescence at both emission wavelengths was measured next to each fiber tested and was then subtracted from all measurements. Fluorescence signals were acquired at a sampling frequency of 50 kHz. The standard ratio method was used with the parameters $R = F405/F485$, R_{min} , R_{max} , K_D , and β having their usual definitions. Results were either expressed in terms of indo-1 percent saturation or in actual free Ca^{2+} concentration. In-cell values for R_{min} , R_{max} , and β used were 0.3, 1.61, and 2, respectively. K_D was assumed to be 350 nM. No correction was made for indo-1- Ca^{2+} binding and dissociation kinetics. The displayed Ca^{2+} signals traces were smoothed using adjacent averaging of a number of datapoints specified in figure legends. Frequencies inducing 50 and 95% fusion of indo-1 and Ca^{2+} signals during train of action potentials (Figs. 5 and 6) were determined graphically in each fiber by fitting a linear function on datapoints between 10 and 70% fusion and a parabolic function on the three datapoints with the highest fusion percentage.

Solutions

The dialyzed intracellular solution contained (in mM) 140 K-glutamate, 5 Na_2 -ATP, 5 Na_2 -phosphocreatine, 5.5 $MgCl_2$, 5 glucose, and 5 HEPES, adjusted to pH 7.2 with KOH, except for the experiments devoted to the measurement of intramembrane charge movements (Fig. 2), for which the dialyzed intracellular solution contained (in mM) 140 Cs-aspartate, 5 Mg-ATP, 1 $MgCl_2$, 10 EGTA-CsOH, and 5 HEPES. The Tyrode solution used in current-clamp conditions contained (in mM) 140 NaCl, 5 KCl, 2.5 $CaCl_2$, 2 $MgCl_2$, and 10 HEPES, adjusted to pH 7.2 with NaOH. The extracellular solution used for measurements of charge movements and Ca^{2+} signals in voltage-clamp conditions contained (in mM) 140 TEA-methanesulphonate, 2.5 $CaCl_2$, 2 $MgCl_2$, 1 4AP, 0.002 TTX, and 10 HEPES, adjusted to pH 7.2. N-benzyl-p-toluene sulphonamide was added in extracellular solutions at 50 μ M.

Statistical analysis

Statistical analysis was performed using Microcal Origin and GraphPad Prism. Least-square fits were performed using a Marquardt–Levenberg algorithm routine included in Microcal Origin. Data are given as means \pm SEM, except for Fig. 6, where data are given as means \pm SD. Normality of data distribution was assessed using Shapiro–Wilk test and statistical differences were determined using a nested *t* test taking into account the number of fibers from each animal as described in Eisner (2021) (left histogram in Fig. 1 C, and Fig. 6, A–G). A Bonferroni correction was used for comparing data in middle and right histograms of Fig. 1 C. For data not normally distributed, statistical differences were determined using unpaired Mann–Whitney–Wilcoxon test (middle and right histograms of Fig. 1 C and Fig. 6 H). Numbers of individual measurements and individual animals used are

mentioned in the figure legends. Differences were considered significant when $P < 0.05$. *, **, and *** indicate $P < 0.05$, $P < 0.005$, and $P < 0.0005$, respectively.

Online supplemental material

Fig. S1 presents indo-1 signals evoked by train of action potentials at increasing frequency in a same zebrafish muscle fiber in order to show that indo-1 fluorescence comes back to a stable resting level between trains. Fig. S2 presents Ca^{2+} changes evoked by 50-Hz trains of action potentials in a zebrafish and in a mouse muscle fiber in order to show the maintained higher level of $[Ca^{2+}]$ after the train in zebrafish.

Results

Action potentials in zebrafish fast muscle fibers

All experiments were performed on muscle fibers isolated from the deep part of adult fish trunk musculature at the level of the dorsal fin. A typical isolated muscle fiber is presented in Fig. 1 A. On average, the fiber length and diameter were 680 ± 64 and 35 ± 0.8 μ m, respectively ($n = 75$). A first series of current clamp experiments showed that these isolated muscle fibers were able to develop action potentials since, in all tested fibers with a membrane potential maintained at -100 mV, injection of 0.5-ms duration suprathreshold depolarizing currents led to the development of action potentials (Fig. 1 B). These data give evidence that the fibers under study were fast type since slow-type fibers were reported to be nonexcitable in zebrafish (Buckingham and Ali, 2004; Luna et al., 2015).

During the course of these experiments, we observed that action potentials displayed overshoot of small amplitude and that the kinetics of the repolarization phase of action potentials was remarkably fast. With the aim of comparing action potential amplitude and kinetics in mouse and zebrafish, we recorded action potentials in isolated mouse and zebrafish skeletal muscle fibers using the same experimental conditions (Fig. 1 B). In average, the maximal amplitude of action potentials was about 30 mV smaller in zebrafish as compared to mouse muscle fibers, and the elapsed time for 20 and 50% repolarization of action potentials after spike was reduced about three- and twofold, respectively, in zebrafish as compared to mouse muscle fibers (Fig. 1 C).

Intramembrane charge movements in zebrafish fast muscle fibers

A next series of experiments aimed at recording the outward membrane currents resulting from the movement of intramembrane charges carried by the $\alpha 1S$ subunit of the DHPR in response to depolarization. Fig. 2 A shows intramembrane charge movements recorded in a voltage-clamped zebrafish muscle fiber in the absence of external Na^+ and K^+ ions and in the presence of Na^+ and K^+ channel blockers and low Cl^- from a holding potential of -80 mV. Membrane currents were detected from -60 mV and increased with depolarization. The density of “on” charges (Q_{on}) was plotted as a function of voltage and fitting the relationship in each cell with a Boltzmann equation gave values for Q_{max} , $V_{0.5}$, and k of 8.8 ± 0.7 nC/ μ F, -32 ± 1.5 mV, and

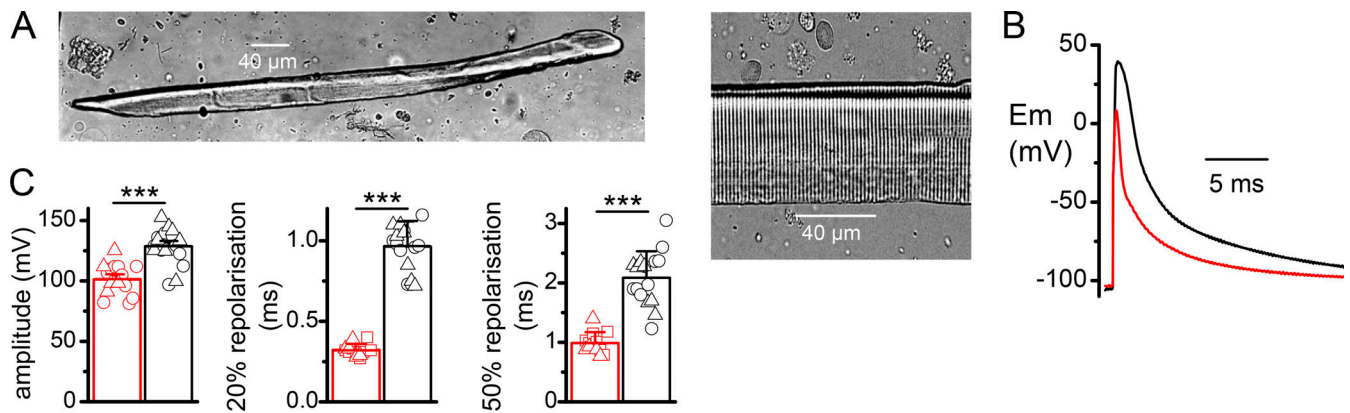


Figure 1. **Isolated adult zebrafish fast skeletal muscle fiber and action potential.** (A) Transmitted light images of an isolated muscle fiber from adult zebrafish at two different magnifications. (B) Action potentials elicited by injection of a 0.5-ms suprathreshold depolarizing current in current clamp conditions in a zebrafish (red) and in a mouse muscle fiber (black). The rising phases have been synchronized for easing comparison. (C) Mean action potential maximal amplitudes and mean elapsed time for 20 and 50% repolarization of action potentials after spike in mouse and zebrafish muscle fibers. The zebrafish and mouse datasets are from 13 fibers from 2 fish and 17 fibers from 2 mice for action potential amplitudes ($P < 0.0001$) and 20% repolarization ($P < 0.0001$) and from 12 fibers from 2 fish and 17 fibers from 2 mice for 50% repolarization ($P = 0.0001$), $***, P < 0.0005$.

9 ± 0.4 mV, respectively (Fig. 2 B). Fig. 2 D also shows that the density of “off” charges (Q_{off}) was very nearly the same as Q_{on} since the best linear fit to Q_{on} datapoints plotted as a function of Q_{off} datapoints for each of the 197 current traces analyzed was

1.1. It has to be noticed that in 13 out of 23 fibers tested, charge movement records exhibited a temporally delayed hump component after the initial peak for depolarizations given between -40 and -20 mV with the maximum hump amplitude at

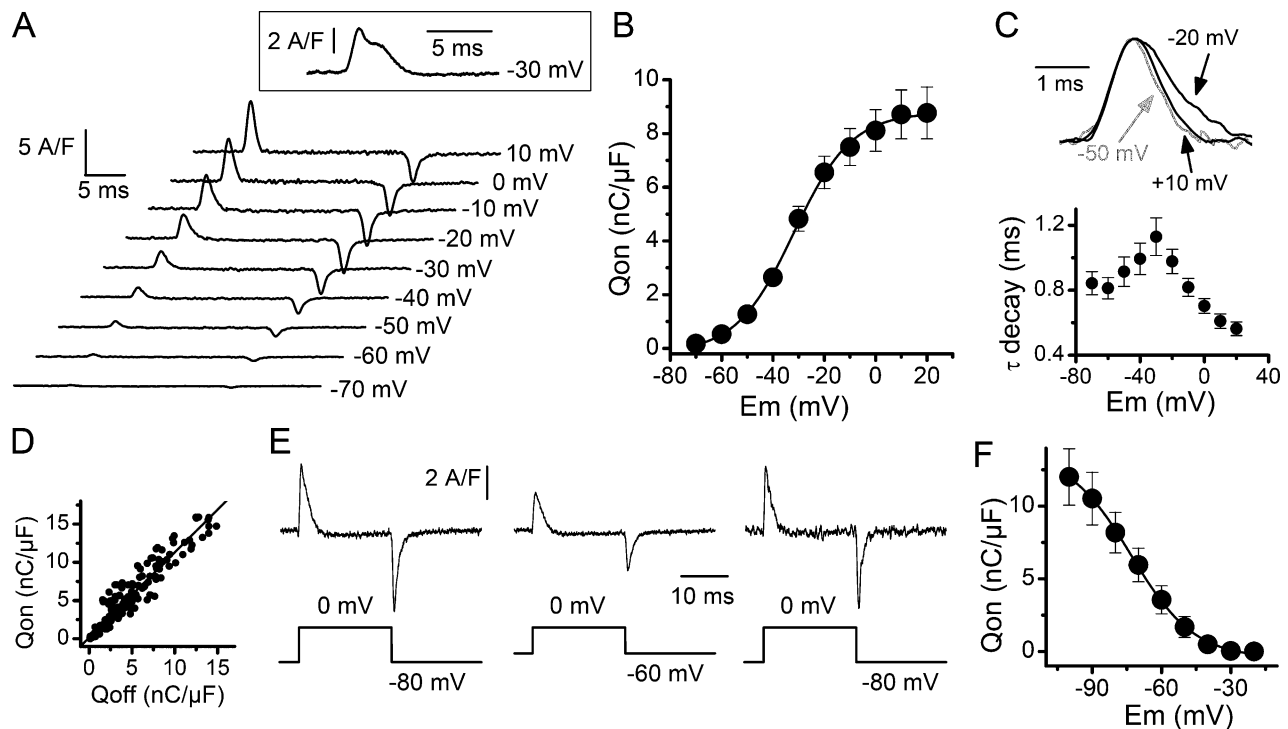


Figure 2. **Intramembrane charge movements evoked by depolarization.** (A) Charge movements records in response to 20-ms-long depolarizing pulses from a holding potential of -80 mV to the indicated values. Inset shows the on outward current displaying a delayed hump component at -30 mV in another fiber. (B) Relationship between the mean density of charge movements (Q_{on}) and membrane potential. Mean datapoints were fitted using a Boltzmann equation with values for Q_{max} , $V_{0.5}$, and k of 8.8 nC/ μ F, -32 mV, and 11 mV, respectively. (C) Superimposition of the on outward current measured in A at the indicated potentials after normalization (upper panel). Relationship between the mean time constant of charge movements decay and membrane potential (lower panel; records displaying a hump have been excluded from the analysis). The mean linear capacitance of the voltage-clamped region of the fibers tested was 586 ± 70 pF. (D) Relationship between Q_{on} and Q_{off} at voltages ranging from -70 to $+20$ mV. Data have been obtained in 23 fibers from 4 fish. (E) Charge movements recorded in the same muscle fiber in response to a voltage pulse to 0 mV from a holding potential of -80 and -60 mV with 20-s time intervals between the pulses. (F) Relationship between Q_{on} recorded in response to a 20-ms voltage pulse to 0 mV and holding potential maintained during 20 s. Data have been obtained in six fibers from one fish.

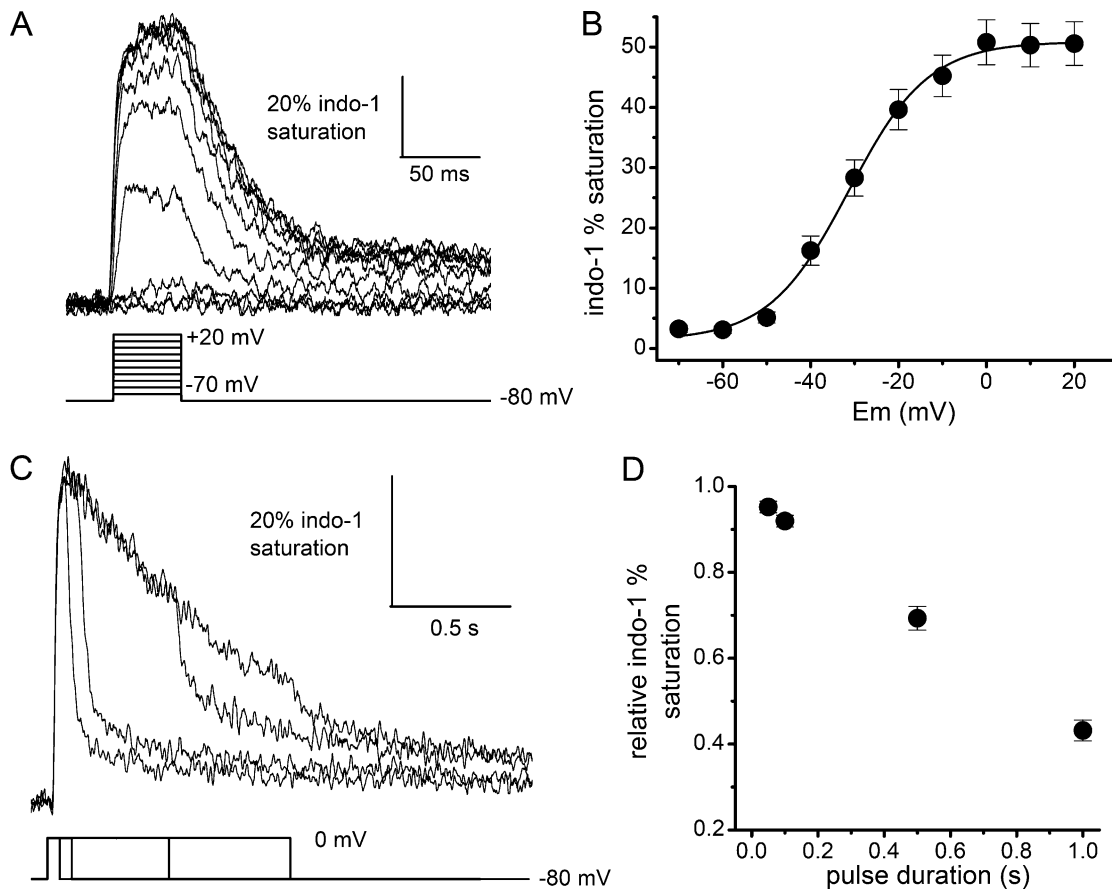


Figure 3. Voltage- and time-dependence of calcium transients elicited by depolarizing pulses. (A) Indo-1 percent saturation traces in response to 50-ms duration depolarizing pulses of increasing amplitude in a same fiber. Traces have been smoothed using adjacent averaging of 20 datapoints. (B) Relationship between mean peak of change in indo-1 percent saturation measured in response to 50-ms depolarization pulses and membrane potential. Mean datapoints were fitted using a Boltzmann equation with values for maximal indo-1 percent saturation, $V_{0.5}$, and k of 51%, -31 and 9 mV, respectively. Data have been obtained in 31 fibers from 6 fish. (C) Indo-1 percent saturation traces in response to depolarizing pulses at 0 mV of increasing duration in a same fiber. Traces have been smoothed using adjacent averaging of 70 datapoints. (D) Mean relative indo-1 percent saturation measured at the end of command pulses, normalized to peak value and plotted as a function of pulse duration. Data have been obtained in 30 fibers from 5 fish.

-32 ± 3 mV (inset of Fig. 2 A). In fibers that did not display this hump, the kinetics of Q_{on} decay were fitted with an exponential function in each fiber for each potential and the mean values of the time constant of charge decay were plotted as a function of membrane potential (Fig. 2 C). The mean time constant of decay was found to increase upon depolarizing the membrane from 0.91 ± 0.09 ms at -50 mV to 1.13 ± 0.12 ms at -30 mV and then decreased to 0.61 ± 0.04 ms at $+10$ mV. Fig. 2 E also shows that the quantity of charges moving in response to a depolarizing pulse to 0 mV was reversibly reduced by depolarizing the holding potential from -80 to -60 mV, indicating that the DHPR undergoes a voltage-dependent inactivation process in response to prolonged depolarization. Plotting the density of intramembrane charge movements as a function of the holding potential and fitting the relationship with a Boltzmann equation indicated that the mean holding potential inducing 50% reduction in charge movements density was -72 ± 1 mV and a steepness factor of 13 ± 1 mV (Fig. 2 F). During the course of these experiments, we also observed that the mean density of charges moving in response to depolarizing pulses given to 0 mV was increased to 12 ± 1.9 nC/ μ F when the holding potential was

brought to -100 mV, indicating that a fraction of DHPRs stands in an inactivated state at -80 mV.

Voltage-dependence of depolarization-induced Ca^{2+} transients in zebrafish fast muscle fibers

By activating the DHPR, depolarization induces the opening of the SR Ca^{2+} release channel that leads to a transient increase in intracellular Ca^{2+} . Using the same external solution as the one used for recording charge movements, intracellular Ca^{2+} transients were measured in response to 50-ms duration depolarizing pulses of increasing amplitudes with the ratiometric Ca^{2+} indicator indo-1 dialyzed into the cells. Depolarizing pulses to voltages above -50 mV induced Ca^{2+} transients which decayed to resting Ca^{2+} level upon repolarization (Fig. 3 A). The amplitude of the Ca^{2+} transients increased with depolarization up to a maximal value reached for depolarizing pulses given above 0 mV. Plotting the maximal amplitude of the Ca^{2+} transient in each cell as a function of voltage and fitting the relationships obtained with a Boltzmann equation gave values for maximal indo-1 percent saturation, $V_{0.5}$, and k of $50 \pm 4\%$, -31 ± 1 mV and 5 ± 1.2 mV, respectively (Fig. 3 B). Fig. 3, D and E shows that prolonging the

duration of the depolarizing pulse to 0 mV induced a progressive decay of the Ca^{2+} transient, reaching in average $43 \pm 2\%$ of the initial amplitude after 1 s.

Inhibition of depolarization-induced Ca^{2+} transients by prepolarization in zebrafish fast muscle fibers

The progressive decay in the amplitude of the Ca^{2+} transients observed with pulse prolongation could be attributed to a progressive closing of the SR Ca^{2+} release channel induced by a voltage- and time-dependent inactivation of the DHPR and to SR Ca^{2+} depletion as described in mouse muscle (Robin and Allard, 2013). The voltage-dependence of the inactivation process was explored by applying 50-ms duration voltage pulses to 0 mV from holding potentials slowly depolarized to incremented voltages and maintained during 20 s, a duration that, on the basis of data collected with the use of SR intraluminal Ca^{2+} dye in mouse muscle, is not long enough to produce SR Ca^{2+} depletion (Robin and Allard, 2013). Fig. 4 A shows that the more depolarized the holding potential, the lower the amplitude of the voltage-evoked Ca^{2+} transient. Plotting the relative amplitude of the Ca^{2+} transients as a function of the holding potential in each cell and fitting the relationships obtained with a Boltzmann equation gave values for $V_{0.5}$ and k of -52 ± 2 , and 5 ± 0.2 mV, respectively (Fig. 4 B). Time-dependence was also investigated by applying a two-pulse protocol consisting of a first pulse of increasing duration given to -45 mV, a value of potential inducing in average between 60 and 80% reduction in Ca^{2+} signals (see Fig. 4 B), followed by a second test pulse of 100-ms duration given to 0 mV. Fig. 4 C shows that the longer the prepulse at -45 mV, the smaller the consecutive Ca^{2+} transient elicited by the test pulse at 0 mV. Plotting the relative amplitude of the Ca^{2+} transients induced by the test pulse as a function of the prepulse duration in each cell and fitting the relationships obtained with a single exponential function indicated a time constant of 0.9 ± 0.2 s (Fig. 4 D). The observed increase in intracellular Ca^{2+} provoked by the pre-depolarizing pulse to -45 mV indicated that the reduction in the Ca^{2+} signal during the test pulse could be due to voltage-dependent inactivation of DHPR plus SR Ca^{2+} depletion.

Ca^{2+} signals induced by trains of action potentials in zebrafish fast muscle fibers

Intracellular Ca^{2+} changes were then investigated in physiological conditions of excitation, i.e., in response to 0.5-s duration trains of action potentials generated in each fiber at increasing frequencies every 15 s. This 15-s interval between trains allowed a full recovery of the basal fluorescence and a maximal amplitude of Ca^{2+} signals which remained stable for all stimulation frequencies in a same fiber (Fig. S1). The left panel of Fig. 5 A shows that single Ca^{2+} transients progressively fused upon increase of the stimulation rate but could still be detected at 20, 50, and 100 Hz and completely fused at 200 Hz stimulation frequency. In order to determine the fusion index of Ca^{2+} transients induced by the stimulation rate, the ratio of the minimum and the maximum values of indo-1 percent saturation of the second Ca^{2+} transient of the train was measured in each cell. Plotting this ratio as a function of the stimulation rate in each cell indicated that half fusion (corresponding to a ratio of 0.5) and 95%

fusion were reached in average at a stimulation frequency of 53 ± 3 and 156 ± 9 Hz respectively (Fig. 6, A and B). When indo-1 signals were converted into intracellular $[\text{Ca}^{2+}]$, the frequency inducing 95% fusion of Ca^{2+} transients was 186 ± 6 Hz (Fig. 6 D).

Comparison of Ca^{2+} signals induced by trains of action potentials in zebrafish and mouse fast muscle fibers

The striking high frequency of Ca^{2+} transients fusion prompted us to record and compare Ca^{2+} transients obtained using the same experimental conditions and protocols in isolated skeletal muscle fibers from mouse interosseal muscle. The right panel of Fig. 5 A shows that indo-1 signals fused at much lower frequencies in mouse muscle, and plotting the fusion index as a function of the stimulation frequency in each cell indicated that half and 95% fusion were reached in average at 20 ± 1 and 62 ± 4 Hz, respectively, values both significantly lower than in zebrafish muscle (Fig. 6, A and B). As a result, the slope of the relationship between fusion index and stimulation frequency was significantly steeper in mouse as compared to zebrafish fibers (Fig. 6 C). When indo-1 signals were converted into intracellular $[\text{Ca}^{2+}]$, the frequency inducing 95% fusion of Ca^{2+} transients in mouse fibers was 92 ± 6 Hz (Fig. 6 D).

A closer look at the single Ca^{2+} transients from mouse and zebrafish fibers during the 20-Hz train led us to deduce that this difference in fusion index resulted from an apparent faster decay of individual indo-1 signals evoked by each action potential in zebrafish fibers. Superimposition of single action potential-evoked indo-1 signals in zebrafish and mouse fibers indeed showed that the decay was faster in zebrafish (Fig. 5 C). Indo-1 signals were then converted into variations in intracellular $[\text{Ca}^{2+}]$ and fitting in each cell $[\text{Ca}^{2+}]$ decay with an exponential function indicated a mean time constant of decay of 8.8 ± 3.4 ms significantly smaller in zebrafish as compared to mouse fibers (Figs. 5 D and 6 E). Additionally, in all zebrafish fibers tested, we never observed any sign of decline of the global Ca^{2+} signal for the entire duration of the stimulation even at the highest stimulation frequency (200 Hz), giving evidence that the fiber was still able to generate action potentials and the SR to release Ca^{2+} with time intervals between stimulations as short as 5 ms (Fig. 5 A, left). In contrast, in mouse muscle, at such a high frequency, only a first Ca^{2+} transient could be evoked in response to the first action potential of the train and then fluorescence went back to baseline (Fig. 5 A, right). When looking at action potentials elicited during the train, it was noticed that the second stimulation of the train failed to trigger an action potential likely because the 5-ms interval was too short to allow membrane repolarization to values enabling recovery of voltage-gated Na^+ channels from inactivation (inset of Fig. 5 A, right, 200 Hz train). The significantly faster repolarization phase of action potentials in zebrafish muscle (see Fig. 1) could explain that zebrafish fibers were still able to fire action potentials at 200 Hz whereas mouse fibers were not.

Two other differences could be also observed between zebrafish and mouse muscle fibers. First, it is clearly visible that, at the end of the stimulus train, the fluorescence signal returned to baseline much slower in zebrafish than in mouse fibers for all stimulation frequencies (Fig. 5). To better appreciate the

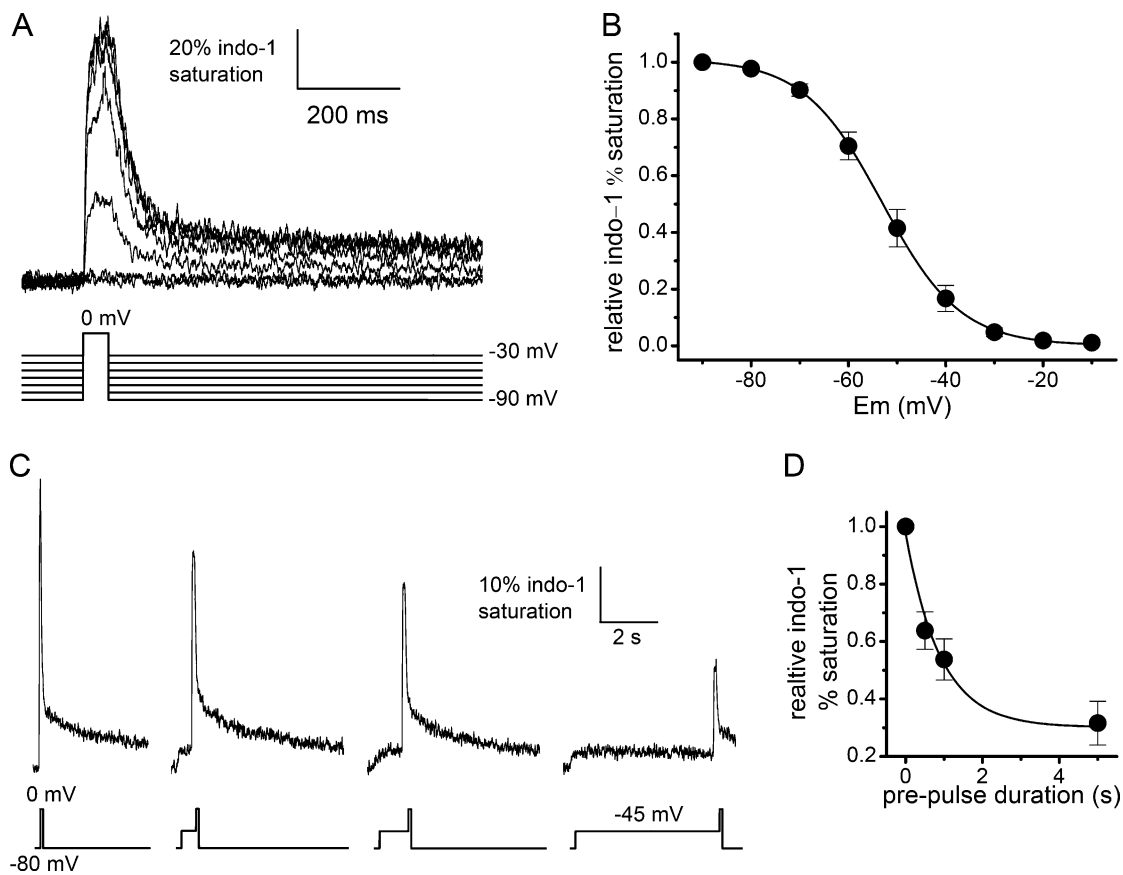


Figure 4. **Inhibition of depolarization-induced Ca^{2+} transients by prepolarization.** (A) Indo-1 signals elicited by 50-ms duration depolarizing pulses at 0 mV from holding potentials increasingly depolarized to the indicated voltages in a same fiber. Traces have been smoothed using adjacent averaging of 20 datapoints. (B) Relationship between mean relative peak of indo-1 percent saturation in response to depolarizing pulses at 0 mV and holding potential. Mean datapoints were fitted using a Boltzmann equation with values for $V_{0.5}$ and k of -53 and 8 mV, respectively. Data have been obtained in 20 fibers from 3 fish. (C) Indo-1 signals elicited by 100-ms duration depolarizing test pulses at 0 mV following a prepulse to -45 mV of increasing duration in a same fiber. Traces have been smoothed using adjacent averaging of 120 datapoints. (D) Relationship between the mean relative decrease in indo-1 signal amplitude during the test pulse and prepulse duration. Datapoints were fitted using a single exponential with a time constant of 0.9 s. Data have been obtained in 16 fibers from 3 fish.

difference in the time course of the Ca^{2+} signal decay after the train between zebrafish and mouse, the fluorescence ratios were converted into Ca^{2+} concentrations and the extent of recovery of the Ca^{2+} signal was measured 300 ms after 50-Hz stimulation trains (Fig. S2). On average, the Ca^{2+} level was significantly larger in zebrafish as compared to mouse fibers (Fig. 6 F). This slower recovery of Ca^{2+} signals in zebrafish fibers was not caused by a higher Ca^{2+} signal amplitude which might have contributed to slowdown the Ca^{2+} signal decay since the mean maximal values of indo-1 signals measured during 50-Hz trains were not significantly different in zebrafish and mouse fibers (Fig. 6 G). Another difference between mouse and zebrafish fibers that could be clearly seen in Fig. 5 A is that the fusion of Ca^{2+} transients significantly increased during the course of the train in zebrafish fibers at 20 and 50 Hz, while it remained fairly stable in mouse fibers. Measuring the changes in the fusion index between the second and the last Ca^{2+} transient during 20 Hz trains in zebrafish and in mouse fibers confirmed that the fusion index increased significantly more markedly in zebrafish as compared to mouse fibers (Fig. 6 H).

Discussion

Our study provides the first comprehensive characterization of EC coupling properties in adult zebrafish fast skeletal muscle fibers. To reach this goal, we were able to combine intracellular Ca^{2+} measurements with current-clamp or voltage-clamp on isolated muscle fibers. In current clamp conditions, we observed that action potentials display a global shape, a spike followed by an early after-potential that was comparable to the shape of action potentials recorded in frog or mammalian muscle fibers under the same experimental conditions (Robin and Allard, 2015; Gage and Eisenberg, 1969). However, we first found that the spike reached in average 0 mV, leading to a mean action potential amplitude 30 mV smaller in zebrafish as compared to mouse muscle fibers. This result is possibly related to a several-orders-of-magnitude lower voltage-gated Na^+ channel current density measured in zebrafish larvae muscle cells as compared to mammalian muscle fibers in extra-junctional regions (Buckingham and Ali, 2004; Caldwell et al., 1986). However, this lower spike amplitude should compromise neither SR Ca^{2+} release, as we showed that full SR Ca^{2+} release could be evoked at

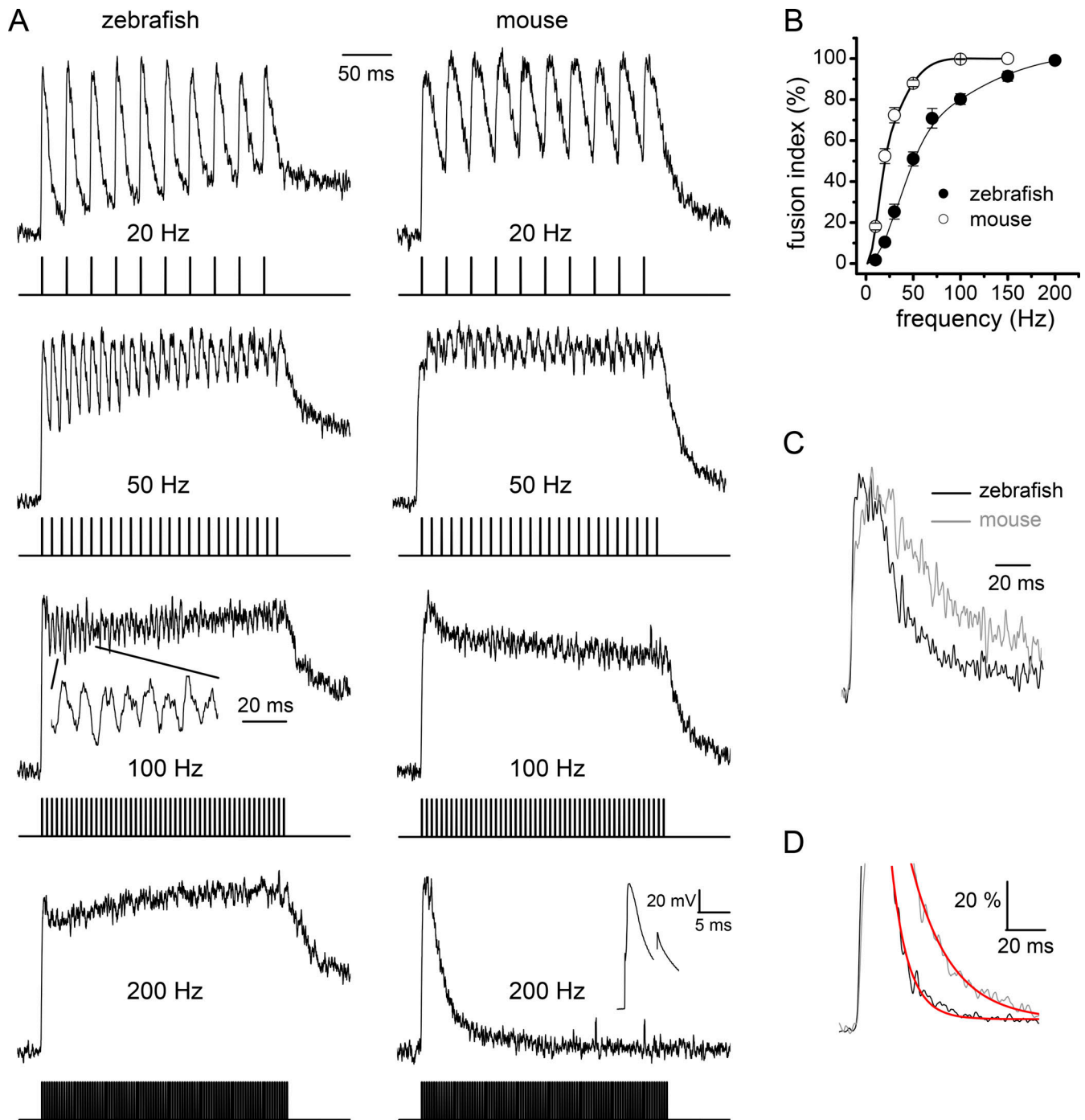


Figure 5. **Action potentials and Ca^{2+} transients evoked by trains of action potentials in zebrafish and mouse muscle fibers.** (A) Normalized indo-1 signals evoked by 0.5-s duration trains of action potentials in response to injection of 0.5-ms duration suprathreshold currents at 20, 50, 100, and 200 Hz in a same zebrafish (left panel) and mouse (right panel) muscle fiber. Traces have been smoothed using adjacent averaging of 100 datapoints. Inset at 100 Hz, left panel, shows the indo-1 signal between 25 and 105 ms after the onset of the train on an expanded scale. Inset at 200 Hz, right panel, shows the changes in membrane potential in response to the first and second suprathreshold stimulation of the 200-Hz train. (B) Relationship between fusion index of indo-1 signals and stimulation frequency in zebrafish and mouse muscle fibers. As an eye guide, the relationships have been fitted with a cubic B-spline smoothing interpolation of the data using the Python SciPy package. Data have been obtained in 17 fibers from 3 fish and 13 fibers from 2 mice. (C) Superimposition of normalized single action potential-evoked indo-1 signals in a mouse and in a zebrafish fiber. Traces have been smoothed using adjacent averaging of 50 datapoints. (D) Indo-1 signals shown in C converted into intracellular $[\text{Ca}^{2+}]$ and normalized. Traces have been smoothed using adjacent averaging of 150 datapoints. The decay phases have been fitted using an exponential function (red traces) with a time constant of 9 and 20 ms for the zebrafish and the mouse signal, respectively.

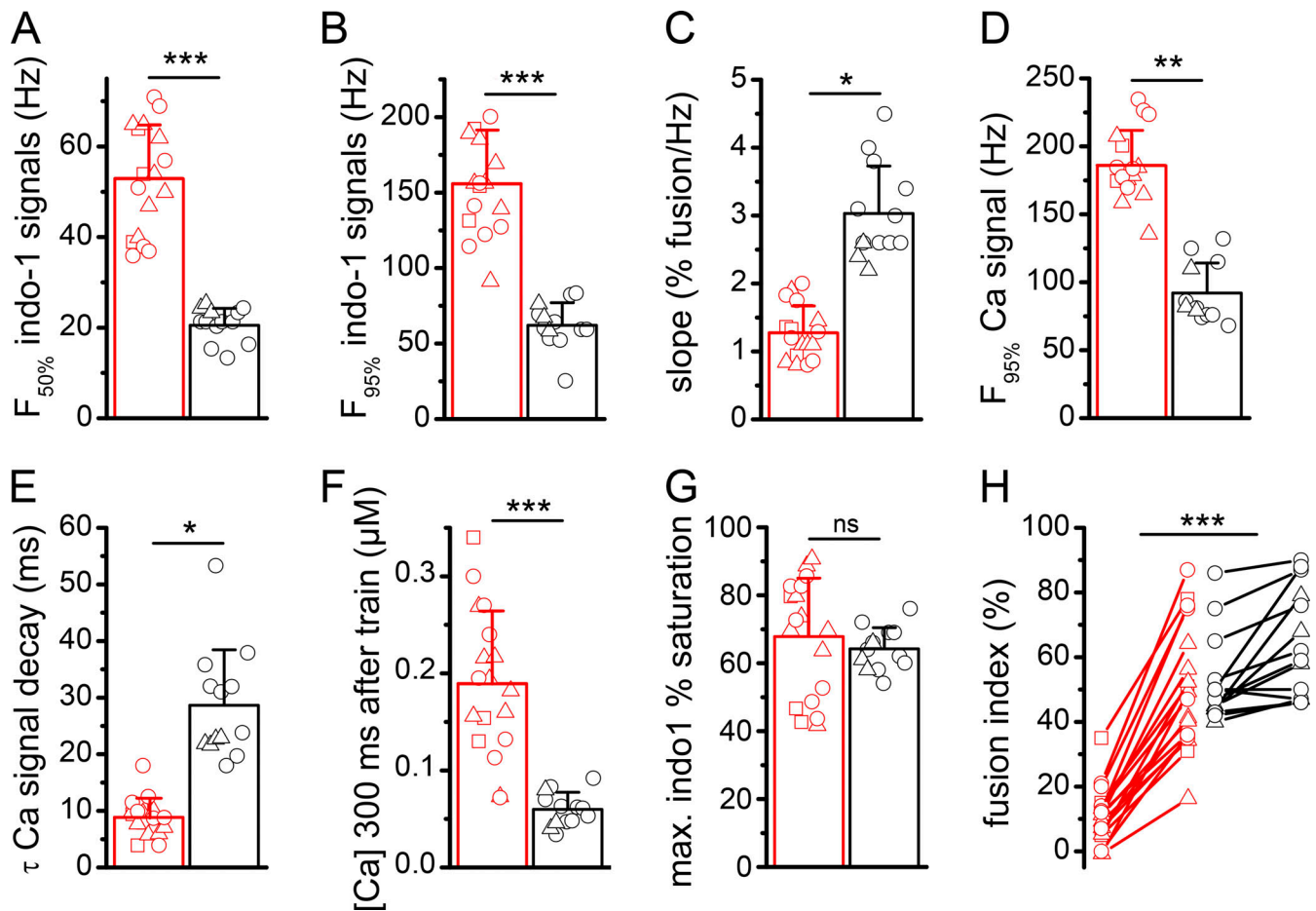


Figure 6. Characteristics of Ca²⁺ transients and action potentials in zebrafish (red) and mouse (black) muscle fibers. (A) Mean stimulation frequencies inducing 50% fusion of indo-1 signals. The zebrafish and mouse datasets are from 17 fibers from 3 fish and 13 fibers from 2 mice ($P < 0.0001$). **(B)** Mean stimulation frequencies inducing 95% fusion of indo-1 signals. The zebrafish and mouse datasets are from 17 fibers from 3 fish and 13 fibers from 2 mice ($P < 0.0001$). **(C)** Mean slope of the relationships between fusion index and stimulation frequencies. The zebrafish and mouse datasets are from 17 fibers from 3 fish and 13 fibers from 2 mice ($P = 0.012$). **(D)** Mean stimulation frequencies inducing 95% fusion of Ca²⁺ transients. The zebrafish and mouse datasets are from 17 fibers from 3 fish and 12 fibers from 2 mice ($P = 0.0047$). **(E)** Mean time constant of decay of single Ca²⁺ transients. The zebrafish and mouse datasets are from 17 fibers from 3 fish and 13 fibers from 2 mice ($P = 0.014$). **(F)** Mean [Ca²⁺] 300 ms after 50-Hz train. The zebrafish and mouse datasets are from 18 fibers from 3 fish and 14 fibers from 2 mice ($P < 0.0001$). **(G)** Mean maximal values of indo-1 percent saturation during 50-Hz train. The zebrafish and mouse datasets are from 17 fibers from 3 fish and 13 fibers from 2 mice. **(H)** Fusion index of the second and the last indo-1 signal within 20-Hz trains. The mean changes in fusion index between the second and the last indo-1 signal have been compared in zebrafish and in mouse fibers. The zebrafish and mouse datasets are from 18 fibers from 3 fish and 14 fibers from 2 mice ($P = 0.0004$). In each panel, individual datapoints from each muscle fiber are presented and data from muscle fibers issued from the same animal are shown with the same symbol. *, $P < 0.05$; **, $P < 0.005$; ***, $P < 0.0005$.

0 mV, nor action potential propagation along the fiber axis since zebrafish fast muscle fibers, in contrast to mouse muscle fibers, are multi-innervated (Luna et al., 2015). By decreasing the metabolic demand of the Na/K ATPase, the reduced Na⁺ influx associated with lower spike amplitude should be concomitantly less costly energetically. A second important finding is that kinetics of the repolarization phase displayed kinetics significantly faster than in mouse skeletal muscle. By considerably shortening the refractory period, this accelerated action potential repolarization allows to preserve fiber excitability up to a 200-Hz frequency of excitation in zebrafish fibers as observed in fast fibers from larvae (Buckingham and Ali, 2004), whereas Na⁺ channel entered in an inactivated state at this frequency after the first action potential in mouse muscle fibers. Interestingly, Dayal et al. (2019) showed in cultured muscle cells from

zebrafish larvae that activation by SR Ca²⁺ release of the Cl⁻ channel ANO1, which is absent in mammalian muscle, is crucial for action potential acceleration. One can postulate that activation of ANO1 is responsible, at least in part, for the fast kinetics of action potential repolarization described here in adult zebrafish muscle.

Kinetics of subsequent steps of activation of the muscle fibers was also found to be strikingly elevated. First, we showed that the kinetics of intramembrane charge movements were faster than those found in mouse muscle. In zebrafish, the dependence of the time constant of charge decay upon membrane potential was bell-shaped, with the time constant reaching maximal value around -30 mV as observed in mouse skeletal muscle, but the mean time constants of decay were lower than those measured in mouse muscle at all membrane potentials (Collet et al., 2003;

Gregorio et al., 2017), and, specifically, about four times lower at the membrane potential inducing maximal time constant. Recently, it has been shown that the four voltage sensors of the $\alpha 1S$ subunit of the DHPR display different kinetics of activation, the fastest being compatible with kinetics of SR Ca^{2+} release whereas the slowest being compatible with Ca^{2+} current activation kinetics (Banks et al., 2021; Savalli et al., 2021). Since the zebrafish DHPR does not conduct Ca^{2+} ions (Schredelseker et al., 2005) and functions as a pure voltage sensor that controls SR Ca^{2+} release channel, it can be suggested that the striking fast charge movements kinetics in zebrafish muscle results from the absence of the slow component of charge movements associated with L-type Ca^{2+} channel opening, all the four voltage sensors being engaged in the fast control of RyR opening. Voltage of half-activation and voltage-dependence steepness of charges in zebrafish muscle were comparable to those found in mouse muscle and, as observed mainly in frog but also in mouse (Csernoch et al., 1991; Prosser et al., 2009), records of charge movements in half of the zebrafish fibers displayed a delayed hump component after the initial peak, possibly related to SR Ca^{2+} release as postulated for frog and mouse. More importantly, the maximal density of charge movements in zebrafish muscle (8.8 and 12 nC/ μ F with a holding potential of -80 and -100 mV, respectively) was half the one reported in mouse skeletal muscle using comparable experimental conditions (Collet et al., 2003). Such a reduced intramembrane charge movements density was also reported in cultured myotubes from zebrafish larvae (Schredelseker et al., 2005; Linsley et al., 2017). This indicates a lower DHPR expression in zebrafish t-tubules but that might be compensated by a higher DHPR–RyR coupling efficacy as postulated by Schrötter et al. (2017) and evidenced in our study by Ca^{2+} signals of comparable amplitude elicited in zebrafish and in mouse muscle fibers in response to trains of action potentials.

Indo-1 calcium transients elicited by controlled membrane depolarizations displayed voltage-dependence of activation in zebrafish muscle fibers comparable to the one recorded in mouse muscle fibers under the same experimental conditions (Collet et al., 1999). The prolongation of depolarization pulses also gave rise to a time-dependent decline of Ca^{2+} signal. Our data obtained with two-pulse protocols on intramembrane charge movements and Ca^{2+} signals ascertain that voltage-activated Ca^{2+} transients in zebrafish muscle undergo a time- and voltage-dependent inactivation process, at least for short duration and low prepolarization values, with mean voltages of half-inhibition and steepness similar to those recorded in mouse muscle (Ursu et al., 2004). Although it was not specifically explored, for higher voltages and/or duration, SR Ca^{2+} depletion may add to voltage-dependent inactivation of DHPR as observed in mouse muscle (Robin and Allard, 2013).

A series of current clamp experiments allowed us to investigate Ca^{2+} signals evoked by trains of action potentials of increasing frequencies in zebrafish fast muscle fibers. Single Ca^{2+} transients elicited by action potentials were found to display striking fast kinetics, so that in response to trains of action potentials, indo-1 signals fused at high frequencies, half fusion, and 95% fusion being observed at 53 and 156 Hz, respectively. These values are obviously dependent on the binding kinetics of the

here-used indo-1 Ca^{2+} dye and, as such, might be underestimated. However, the value of 186 Hz obtained for 95% fusion after conversion into $[Ca^{2+}]$ is very consistent with the 190 Hz stimulation frequency required to induce full fusion of twitches during tetanic contraction in zebrafish larvae muscle (Dou et al., 2008). These fusion frequencies are also close to the one reported for the fastest muscle known among vertebrate muscles, the muscles from toadfish swim bladder that produce sounds at the frequency at which the muscles contract (150–200 Hz at $16^{\circ}C$; Rome et al., 1996). Along this line, swim bladder muscle fibers injected with the Ca^{2+} dye fluo-4, which has binding kinetics comparable to indo-1, were shown to exhibit decay kinetics of Ca^{2+} transients elicited by action potentials and degree of fusion of individual Ca^{2+} transients at a stimulation frequency of 83 Hz comparable to those that we measured for zebrafish fast muscle fibers (see Fig. 4 in Nelson et al. [2014]). Above all, we found that decay kinetics of action potential-evoked Ca^{2+} transients were significantly faster in zebrafish fibers as compared to fibers isolated from mouse interosseal muscle, composed of type IIa fibers (Friedrich et al., 2008), suggesting a higher activity and/or density of SR Ca^{2+} pumps in zebrafish muscle fibers. Consequently, half and full fusion of Ca^{2+} transients occurred at stimulation frequencies significantly much higher than those found in mouse muscle fibers. Additionally, whereas fused Ca^{2+} transients at 200 Hz were maintained during the entire duration of the tetanic stimulation in zebrafish fibers, Ca^{2+} signal faded away after the first Ca^{2+} transient in mouse muscle fibers because of progressive membrane refractoriness provoked by the short 5-ms repolarization interval. Yet, adult zebrafish muscle fibers express the RyR type 1 (RyR1) and type 3 (RyR3) isoform at the same level, and this latter was shown to contribute to prolong Ca^{2+} transients in frog muscle (Darbandi and Franck, 2009; Hollingworth and Baylor, 2013). In muscle fibers from zebrafish larvae, RyR3 was also demonstrated to be present, but, in contrast to frog, action potential-evoked Ca^{2+} transients displayed comparable kinetics as shown here for adult zebrafish muscle (Perni et al., 2014; Xiyuan et al., 2017). Concomitantly, silencing of RyR3 expression by morpholino injection in zebrafish larvae did not induce any reduction in the tail-flip response of the fish (Perni et al., 2014). These data obtained in larvae and our present work may indicate that RyR3 did not significantly contribute to action potential-evoked SR Ca^{2+} release and its role remains to be elucidated.

An unforeseen observation was that the recovery of the Ca^{2+} signal following a train of action potentials was much slower in zebrafish as compared to mouse muscle fibers. Such a slowdown of Ca^{2+} decay was also observed in superfast muscle fibers from swim bladder after a high frequency train of action potentials of the same 0.5-s duration (Nelson et al., 2014). In swim bladder muscle, this reduced declining rate was attributed to the slow unbinding of Ca^{2+} from the high affinity metal-binding sites of the protein parvalbumin, the intracellular concentration of which is three to four times higher in swim bladder muscle fibers as compared to mouse fast muscle fibers. It is thus very likely that the reduced rate of Ca^{2+} decay mainly results from the slower release of Ca^{2+} from parvalbumin or other high affinity intracellular Ca^{2+} buffer binding sites at higher density in

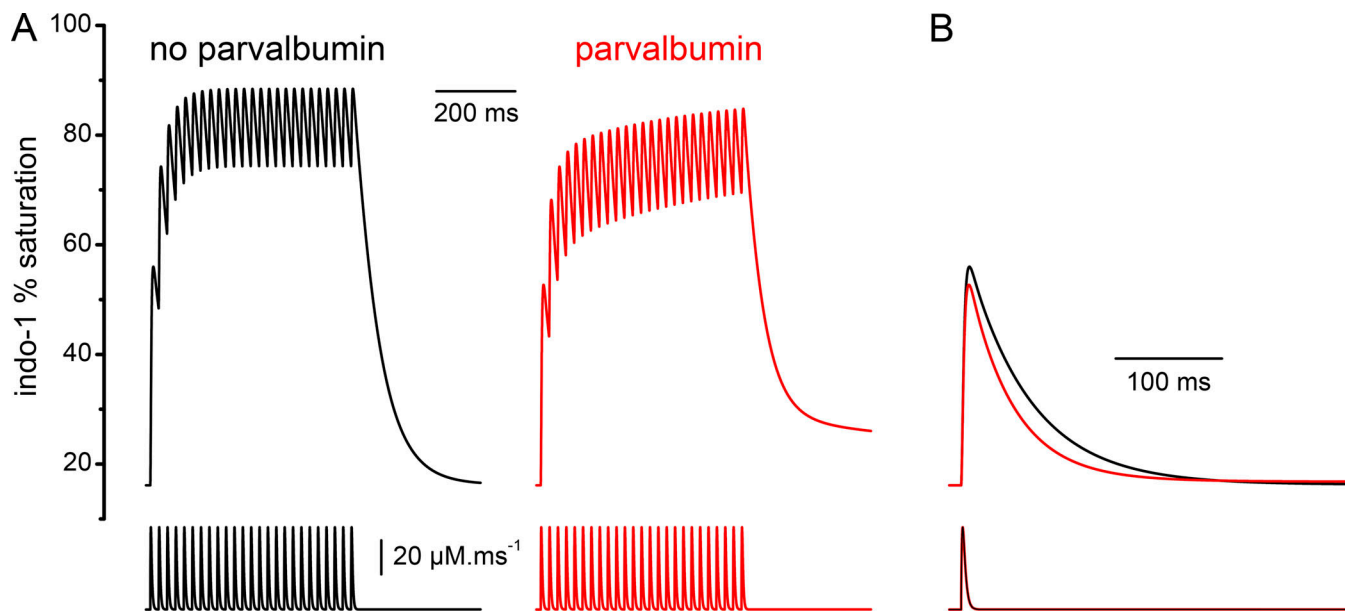


Figure 7. Simulation of the effect of parvalbumin Ca^{2+} -binding sites on the indo-1 transients generated by 50-Hz train and single Ca^{2+} release pulses. The waveform of release shown at the bottom was used to calculate the above indo-1 percent saturation traces assuming either absence (black) or presence of parvalbumin binding sites at a concentration of 3 mM (red). **(A and B)** The synthetic Ca^{2+} release waveform was set as a 50-Hz train (A) or a single (B) arbitrarily defined peaks of $50\text{-}\mu\text{M}\cdot\text{ms}^{-1}$ amplitude with a half-width of ~ 4 ms. The model included binding sites for troponin C, parvalbumin, and the SR pump. Values for parameters were taken from [Sanchez et al. \(2021\)](#), except for the maximum SR pump rate which was set to $20\text{ }\mu\text{M}\cdot\text{ms}^{-1}$ and for the Ca^{2+} -dye binding properties which were set to those measured for indo-1 by [Jackson et al. \(1987\)](#).

zebrafish as compared to mouse muscle. In agreement with this interpretation, we found that fusion of Ca^{2+} transients increased much more strongly during the course of the stimulation train in zebrafish than in mouse muscle, likely because of a progressive slow binding of Ca^{2+} on Ca^{2+} buffers. [Nelson et al. \(2014\)](#) proposed that a large concentration of parvalbumin and of SR Ca^{2+} pumps in swim bladder muscle enables a quick fall of the Ca^{2+} concentration to a level where there is no activation of the contractile proteins, but above the resting level to permit Ca^{2+} pumping at rates substantially above the resting pump rate allowing in this way superfast cycles of SR Ca^{2+} release and pumping. We suggest that comparable mechanisms underlie the ability of the zebrafish fast muscle fibers to generate high frequency bursts of Ca^{2+} transients since intracellular $[\text{Ca}^{2+}]$ was also found to fall to mean levels (190 nM) above resting concentration but likely below contractile threshold. In accordance with these presumptions, we were able to reproduce the differential features of the measured zebrafish transients versus those of the mouse by using a model including or not a cytosolic buffer. The combined effect of a fast removal system and a cytosolic buffer with the kinetics of parvalbumin was simulated using a synthetic waveform of Ca^{2+} release set as a 50-Hz train of arbitrarily defined peaks and fed into a calcium distribution model, as previously described ([Collet and Jacquemond, 2002](#); [Pouvreau et al., 2006](#)). The corresponding calculated changes in indo-1 percent saturation clearly show that the inclusion of parvalbumin sites qualitatively reproduces a progressive accumulation of the inter-transient level and a reduced rate of decay at the end of the train ([Fig. 7 A](#)). [Fig. 7 B](#) also shows that the calculated changes in indo-1 percent saturation generated

by a single Ca^{2+} release pulse display faster decay kinetics in the presence of parvalbumin, again suggesting that the presence of a cytosolic buffer at higher concentration in zebrafish could explain the differences in single action potential evoked indo-1 signals observed between mouse and zebrafish ([Fig. 5 C](#)).

To our knowledge, our study is the first demonstration of superfast properties of EC coupling in vertebrate skeletal muscles involved in locomotion. Kinetics of each step of EC coupling turned out to be strikingly elevated, from action potential, intramembrane charge movements, to Ca^{2+} transients. Together with low Ca^{2+} sensitivity of contractile proteins ([Dou et al., 2008](#)), this superfast EC coupling enables superfast contraction kinetics of zebrafish fast muscle fibers that are known to be involved in the startle response of the animal ([Buss and Drapeau, 2001](#); [Müller and van Leeuwen, 2004](#); [Kyriakatos et al., 2011](#)). Superfast contraction kinetics obviously also require superfast myosins. In addition to zebrafish fast skeletal muscle, superfast myosins have been identified in sonic muscles from swim bladder but also in masticatory jaw muscles from mammals that have been shown to display contraction kinetics comparable to zebrafish trunk muscles ([Taylor et al., 1973](#); [Hoh, 2002](#); [Mead et al., 2020](#)). In a phylogenetical point of view, the euteleost zebrafish is more advanced than mammals and it is likely that the fish developed these superfast locomotor behaviors critical for evading predators and capturing preys. In providing a comprehensive characterization of EC coupling properties in zebrafish fast muscle fibers, this study should also serve as a reference database to improve and optimize the use of the zebrafish model at adult stage for a better understanding of the

physiological mechanisms involved not only in muscle disorders but also in normal muscle function.

Acknowledgments

Eduardo Ríos served as editor.

This work was supported by the Université Claude Bernard Lyon 1, the Centre National de la Recherche Scientifique (CNRS), l'Institut National de la Santé et de Recherche Médicale (INSERM), l'Association Française contre les Myopathies (AFM-Téléthon—Alliance MyoNeurALP2, project 4.1.1), la Fondation pour la Recherche Médicale (FRM, project ECO201806006866), and the ANR (Agence Nationale de la Recherche, project FishandCol6).

The authors declare no competing financial interests.

Author contributions: R. Idoux designed, performed and analyzed data. C. Berthier, S. Breteau, F. Ruggiero and V. Jacquemond gave conceptual advice. V. Jacquemond generated the model simulating indo-1 signals. B. Allard designed experiments, analyzed data, and wrote the paper.

Submitted: 21 March 2022

Accepted: 15 June 2022

References

- Allard, B. 2018. From excitation to intracellular Ca^{2+} movements in skeletal muscle: Basic aspects and related clinical disorders. *Neuromuscul. Disord.* 28:394–401. <https://doi.org/10.1016/j.nmd.2018.03.004>
- Banks, Q., H. Bibollet, M. Contreras, D.F. Bennett, R.A. Bannister, M.F. Schneider, and E.O. Hernández-Ochoa. 2021. Voltage sensor movements of $Ca_v1.1$ during an action potential in skeletal muscle fibers. *Proc. Natl. Acad. Sci. USA.* 118:e2026116118. <https://doi.org/10.1073/pnas.2026116118>
- Baylor, S.M., and S. Hollingworth. 2012. Intracellular calcium movements during excitation-contraction coupling in mammalian slow-twitch and fast-twitch muscle fibers. *J. Gen. Physiol.* 139:261–272. <https://doi.org/10.1085/jgp.201210773>
- Berger, J., and P.D. Currie. 2012. Zebrafish models flex their muscles to shed light on muscular dystrophies. *Dis. Model. Mech.* 5:726–732. <https://doi.org/10.1242/dmm.010082>
- Buckingham, S.D., and D.W. Ali. 2004. Sodium and potassium currents of larval zebrafish muscle fibres. *J. Exp. Biol.* 207:841–852. <https://doi.org/10.1242/jeb.00839>
- Buss, R.R., and P. Drapeau. 2001. Synaptic drive to motoneurons during fictive swimming in the developing zebrafish. *J. Neurophysiol.* 86:197–210. <https://doi.org/10.1152/jn.2001.86.1.197>
- Caldwell, J.H., D.T. Campbell, and K.G. Beam. 1986. Na channel distribution in vertebrate skeletal muscle. *J. Gen. Physiol.* 87:907–932. <https://doi.org/10.1085/jgp.87.6.907>
- Collet, C., B. Allard, Y. Tourneur, and V. Jacquemond. 1999. Intracellular calcium signals measured with indo-1 in isolated skeletal muscle fibres from control and *mdx* mice. *J. Physiol.* 520 Pt 2:417–429. <https://doi.org/10.1111/j.1469-7793.1999.00417.x>
- Collet, C., and V. Jacquemond. 2002. Sustained release of calcium elicited by membrane depolarization in ryanodine-injected mouse skeletal muscle fibres. *Biophys. J.* 82:1509–1523. [https://doi.org/10.1016/S0006-3495\(02\)75504-5](https://doi.org/10.1016/S0006-3495(02)75504-5)
- Collet, C., L. Csernoch, and V. Jacquemond. 2003. Intramembrane charge movement and L-type calcium current in skeletal muscle fibers isolated from control and *mdx* mice. *Biophys. J.* 84:251–265. [https://doi.org/10.1016/S0006-3495\(03\)74846-2](https://doi.org/10.1016/S0006-3495(03)74846-2)
- Csernoch, L., G. Pizarro, I. Uribe, M. Rodríguez, and E. Ríos. 1991. Interfering with calcium release suppresses I_T , the “hump” component of intramembranous charge movement in skeletal muscle. *J. Gen. Physiol.* 97:845–884. <https://doi.org/10.1085/jgp.97.5.845>
- Darbandi, S., and J.P.C. Franck. 2009. A comparative study of ryanodine receptor (RyR) gene expression levels in a basal ray-finned fish, bichir

- (*Polypterus ornatipinnis*) and the derived euteleost zebrafish (*Danio rerio*). *Comp. Biochem. Physiol. B Biochem. Mol. Biol.* 154:443–448. <https://doi.org/10.1016/j.cbpb.2009.09.003>
- Dayal, A., S.F.J. Ng, and M. Grabner. 2019. Ca^{2+} -activated Cl^- channel TMEM16A/ANO1 identified in zebrafish skeletal muscle is crucial for action potential acceleration. *Nat. Commun.* 10:115. <https://doi.org/10.1038/s41467-018-07918-z>
- Dou, Y., M. Andersson-Lendahl, and A. Arner. 2008. Structure and function of skeletal muscle in zebrafish early larvae. *J. Gen. Physiol.* 131:445–453. <https://doi.org/10.1085/jgp.200809982>
- Eisner, D.A. 2021. Pseudoreplication in physiology: More means less. *J. Gen. Physiol.* 153:e202012826. <https://doi.org/10.1085/jgp.202012826>
- Friedrich, O., C. Weber, F. von Wegner, J.S. Chamberlain, and R.H. Fink. 2008. Unloaded speed of shortening in voltage-clamped intact skeletal muscle fibers from wt, *mdx*, and transgenic minidystrophin mice using a novel high-speed acquisition system. *Biophys. J.* 94:4751–4765. <https://doi.org/10.1529/biophysj.107.126557>
- Gage, P.W., and R.S. Eisenberg. 1969. Action potentials, afterpotentials, and excitation-contraction coupling in frog sartorius fibers without transverse tubules. *J. Gen. Physiol.* 53:298–310. <https://doi.org/10.1085/jgp.53.3.298>
- Gibbs, E.M., E.J. Horstick, and J.J. Dowling. 2013. Swimming into prominence: The zebrafish as a valuable tool for studying human myopathies and muscular dystrophies. *FEBS J.* 280:4187–4197. <https://doi.org/10.1111/febs.12412>
- Gregorio, J.F., G. Pequera, C. Manno, E. Ríos, and G. Brum. 2017. The voltage sensor of excitation-contraction coupling in mammals: Inactivation and interaction with Ca^{2+} . *J. Physiol.* 149:1041–1058. <https://doi.org/10.1085/jgp.201611725>
- Guyon, J.R., L.S. Steffen, M.H. Howell, T.J. Pusack, C. Lawrence, and L.M. Kunkel. 2007. Modeling human muscle disease in zebrafish. *Biochim. Biophys. Acta.* 1772:205–215. <https://doi.org/10.1016/j.bbadis.2006.07.003>
- Hoh, J.F.Y. 2002. “Superfast” or masticatory myosin and the evolution of jaw-closing muscles of vertebrates. *J. Exp. Biol.* 205:2203–2210. <https://doi.org/10.1242/jeb.205.15.2203>
- Hollingworth, S., and S.M. Baylor. 2013. Comparison of myoplasmic calcium movements during excitation-contraction coupling in frog twitch and mouse fast-twitch muscle fibers. *J. Gen. Physiol.* 141:567–583. <https://doi.org/10.1085/jgp.201310961>
- Idoux, R., C. Fuster, V. Jacquemond, A. Dayal, M. Grabner, P. Charnet, and B. Allard. 2020. Divalent cations permeation in a Ca^{2+} non-conducting skeletal muscle dihydropyridine receptor mouse model. *Cell Calcium.* 91:102256. <https://doi.org/10.1016/j.ceca.2020.102256>
- Jackson, A.P., M.P. Timmerman, C.R. Bagshaw, and C.C. Ashley. 1987. The kinetics of calcium binding to fura-2 and indo-1. *FEBS Lett.* 216:35–39. [https://doi.org/10.1016/0014-5793\(87\)80752-4](https://doi.org/10.1016/0014-5793(87)80752-4)
- Kyriakatos, A., R. Mahmood, J. Ausborn, C.P. Porres, A. Büschges, and A. El Manira. 2011. Initiation of locomotion in adult zebrafish. *J. Neurosci.* 31:8422–8431. <https://doi.org/10.1523/JNEUROSCI.1012-11.2011>
- Linsley, J.W., I.U. Hsu, L. Groom, V. Yarotsky, M. Lavorato, E.J. Horstick, D. Linsley, W. Wang, C. Franzini-Armstrong, R.T. Dirksen, and J.Y. Kuwada. 2017. Congenital myopathy results from misregulation of a muscle Ca^{2+} channel by mutant Stac3. *Proc. Natl. Acad. Sci. USA.* 114:228–236. <https://doi.org/10.1073/pnas.1619238114>
- Luna, V.M., E. Daikoku, and F. Ono. 2015. “Slow” skeletal muscles across vertebrate species. *Cell Biosci.* 5:62. <https://doi.org/10.1186/s13578-015-0054-6>
- Mead, A.F., G.G. Kennedy, B.M. Palmer, A.M. Ebert, and D.M. Warshaw. 2020. Mechanical characteristics of ultrafast zebrafish larval swimming muscles. *Biophys. J.* 119:806–820. <https://doi.org/10.1016/j.bpj.2020.06.036>
- Melzer, W., A. Herrmann-Frank, and H.C. Lüttgau. 1995. The role of Ca^{2+} ions in excitation-contraction coupling of skeletal muscle fibres. *Biochim. Biophys. Acta.* 1241:59–116. [https://doi.org/10.1016/0304-4157\(94\)00014-5](https://doi.org/10.1016/0304-4157(94)00014-5)
- Müller, U.K., and J.L. van Leeuwen. 2004. Swimming of larval zebrafish: Ontogeny of body waves and implications for locomotory development. *J. Exp. Biol.* 207:853–868. <https://doi.org/10.1242/jeb.00821>
- Nelson, F.E., S. Hollingworth, L.C. Rome, and S.M. Baylor. 2014. Intracellular calcium movements during relaxation and recovery of superfast muscle fibers of the toadfish swimbladder. *J. Gen. Physiol.* 143:605–620. <https://doi.org/10.1085/jgp.201411160>
- Parichy, D.M., M.R. Elizondo, M.G. Mills, T.N. Gordon, and R.E. Engeszer. 2009. Normal table of postembryonic zebrafish development: Staging

- by externally visible anatomy of the living fish. *Dev. Dyn.* 238: 2975–3015. <https://doi.org/10.1002/dvdy.22113>
- Perni, S., K.C. Marsden, M. Escobar, S. Hollingworth, S.M. Baylor, and C. Franzini-Armstrong. 2015. Structural and functional properties of ryanodine receptor type 3 in zebrafish tail muscle. *J. Gen. Physiol.* 145:253. <https://doi.org/10.1085/jgp.20141130302112015c>
- Pouvreau, S., L. Csernoch, B. Allard, J.M. Sabatier, M. De Waard, M. Ronjat, and V. Jacquemond. 2006. Transient loss of voltage control of Ca²⁺ release in the presence of maurocalcine in skeletal muscle. *Biophys. J.* 91: 2206–2215. <https://doi.org/10.1529/biophysj.105.078089>
- Prosser, B.L., E.O. Hernández-Ochoa, D.B. Zimmer, and M.F. Schneider. 2009. The Qgamma component of intra-membrane charge movement is present in mammalian muscle fibres, but suppressed in the absence of S100A1. *J. Physiol.* 587:4523–4541. <https://doi.org/10.1113/jphysiol.2009.177238>
- Rios, E., and G. Pizarro. 1991. Voltage sensor of excitation-contraction coupling in skeletal muscle. *Physiol. Rev.* 71:849–908. <https://doi.org/10.1152/physrev.1991.71.3.849>
- Robin, G., and B. Allard. 2013. Major contribution of sarcoplasmic reticulum Ca²⁺ depletion during long-lasting activation of skeletal muscle. *J. Gen. Physiol.* 141:557–565. <https://doi.org/10.1085/jgp.201310957>
- Robin, G., and B. Allard. 2015. Voltage-gated Ca²⁺ influx through L-type channels contributes to sarcoplasmic reticulum Ca²⁺ loading in skeletal muscle. *J. Physiol.* 593:4781–4797. <https://doi.org/10.1113/JP270252>
- Rome, L.C. 2006. Design and function of superfast muscles: New insights into the physiology of skeletal muscle. *Annu. Rev. Physiol.* 68:193–221. <https://doi.org/10.1146/annurev.physiol.68.040104.105418>
- Rome, L.C., D.A. Syme, S. Hollingworth, S.L. Lindstedt, and S.M. Baylor. 1996. The whistle and the rattle: The design of sound producing muscles. *Proc. Natl. Acad. Sci. USA.* 93:8095–8100. <https://doi.org/10.1073/pnas.93.15.8095>
- Sanchez, C., C. Berthier, Y. Tourneur, L. Monteiro, B. Allard, L. Csernoch, and V. Jacquemond. 2021. Detection of Ca²⁺ transients near ryanodine receptors by targeting fluorescent Ca²⁺ sensors to the triad. *J. Gen. Physiol.* 153:e202012592. <https://doi.org/10.1085/jgp.202012592>
- Savalli, N., M. Angelini, F. Steccanella, J. Wier, F. Wu, M. Quinonez, M. Di-Franco, A. Neely, S.C. Cannon, and R. Olcese. 2021. The distinct role of the four voltage sensors of the skeletal CaV1.1 channel in voltage-dependent activation. *J. Gen. Physiol.* 153:e202112915. <https://doi.org/10.1085/jgp.202112915>
- Schneider, M.F. 1994. Control of calcium release in functioning skeletal muscle fibers. *Annu. Rev. Physiol.* 56:463–484. <https://doi.org/10.1146/annurev.ph.56.030194.002335>
- Schiaffino, S., and C. Reggiani. 2011. Fiber types in mammalian skeletal muscles. *Physiol. Rev.* 91:1447–1531. <https://doi.org/10.1152/physrev.00031.2010>
- Schredelseker, J., V. Di Biase, G.J. Obermair, E.T. Felder, B.E. Flucher, C. Franzini-Armstrong, and M. Grabner. 2005. The beta 1a subunit is essential for the assembly of dihydropyridine-receptor arrays in skeletal muscle. *Proc. Natl. Acad. Sci. USA.* 102:17219–17224. <https://doi.org/10.1073/pnas.0508710102>
- Schrötter, K., A. Dayal, and M. Grabner. 2017. The mammalian skeletal muscle DHP has larger Ca²⁺ conductance and is phylogenetically ancient to the early ray finned fish sterlet (*Acipenser ruthenus*). *Cell Calcium.* 61:22–31. <https://doi.org/10.1016/j.ceca.2016.10.002>
- Taylor, A., F.W. Cody, and M.A. Bosley. 1973. Histochemical and mechanical properties of the jaw muscles of the cat. *Exp. Neurol.* 38:99–109. [https://doi.org/10.1016/0014-4886\(73\)90011-3](https://doi.org/10.1016/0014-4886(73)90011-3)
- Ursu, D., R.P. Schuhmeier, M. Freichel, V. Flockerzi, and W. Melzer. 2004. Altered inactivation of Ca²⁺ current and Ca²⁺ release in mouse muscle fibers deficient in the DHP receptor gamma subunit. *J. Gen. Physiol.* 124: 605–618. <https://doi.org/10.1085/jgp.200409168>
- Walogorsky, M., R. Mongeon, H. Wen, G. Mandel, and P. Brehm. 2012. Acetylcholine receptor gating in a zebrafish model for slow-channel syndrome. *J. Neurosci.* 32:7941–7948. <https://doi.org/10.1523/JNEUROSCI.0158-12.2012>
- Xiyuan, Z., R.H.A. Fink, and M. Mosqueira. 2017. NO-sGC Pathway modulates Ca²⁺ release and muscle contraction in zebrafish skeletal muscle. *Front. Physiol.* 8:607. <https://doi.org/10.3389/fphys.2017.00607>

Supplemental material

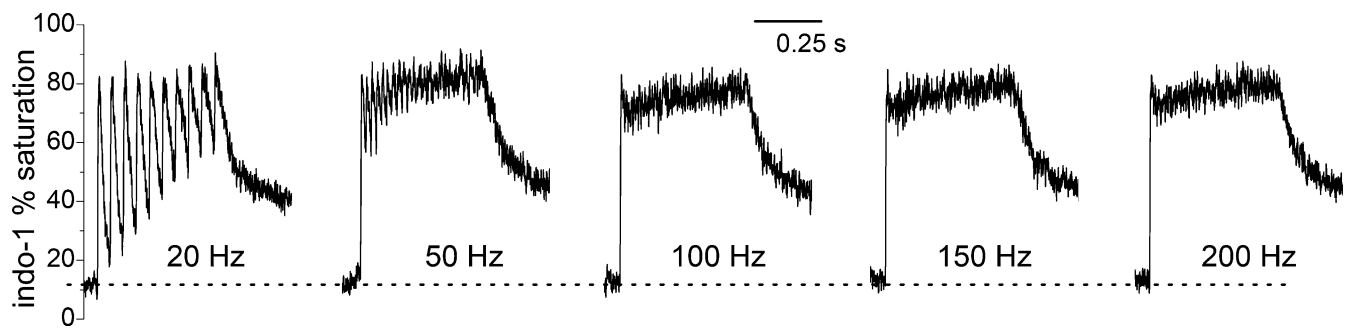


Figure S1. **Indo-1 signals evoked by train of action potentials in response to injection of 0.5-ms duration suprathreshold currents at 20, 50, 100, 150, and 200 Hz every 15 s in a same zebrafish muscle fiber.** Traces have been smoothed using adjacent averaging of 100 datapoints. Note that indo-1 fluorescence comes back to a stable resting level between trains.

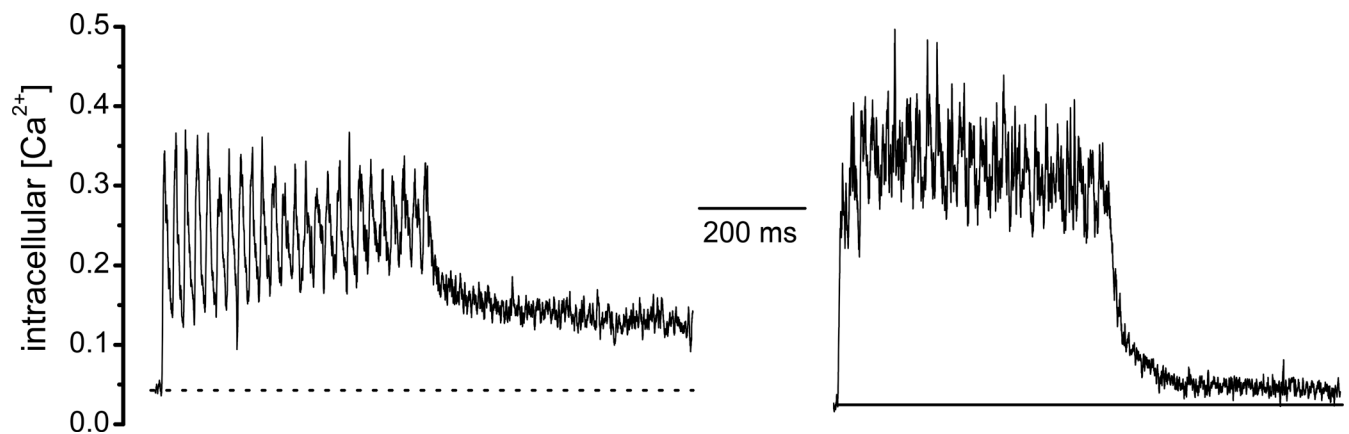


Figure S2. **Comparison of Ca^{2+} changes evoked by 50-Hz trains of action potentials in a zebrafish and in a mouse muscle fiber.** Note the maintained higher level of $[\text{Ca}^{2+}]$ after the train in zebrafish.